Univ. of Queensland, Australia, 1994.
[9]Shau, Y. R., and Dolling, D. S., "Exploratory Study of Turbulent Structure of a Compressible Shear Layer Using Fluctuating Pitot Pressure Measurements," *Experiments in Fluids*, Vol. 12, 1992, pp. 293–306.
[10]He, Y., and Morgan, R. G., "Transition of Compressible High Enthalpy Boundary Layer Flow over a Flat Plate," *Aeronautical Journal*, Vol. 98, No. 972, 1994, pp. 25–34.
[11]Brescianini, C. P., "An Investigation of the Wall-Injected Scramjet," Ph.D. Dissertation, Dept. of Mechanical Engineering, Univ. of Queensland, Australia, 1992.
[12]Patankar, S. V., and Spalding, D. B., *Heat and Mass Transfer in Boundary Layers*, 2nd ed., International Textbook, London, 1970.
[13]Elghobashi, S., and Spalding, D. B., "Equilibrium Chemical Reaction of Supersonic Hydrogen-Air Jets (The ALMA Computer Program)," NASA CR-2725, 1977.
[14]Brescianini, C. P., "Modified k-ε Model for Compressible Free Shear Flows," *AIAA Journal*, Vol. 30, No. 8, 1992, pp. 2161–2163.

Combustion of Liquid Oxygen with Hydrogen Under High-Pressure Conditions

An-Shik Yang*
National Space Program Office, Hsin-Chu 300, Taiwan, Republic of China
Wen H. Hsieh†
National Chung-Cheng University, Chia-Yi 621, Taiwan, Republic of China
and
Kenneth K. Kuo‡
Pennsylvania State University, University Park, Pennsylvania 16802

Introduction

LIQUID OXYGEN (LOX) and hydrogen have been used in various types of liquid rocket engines because of their high specific impulse and low exhaust pollution.[1] Numerous flow and chemical complexities involved in the LOX evaporation and combustion processes have attracted significant attention of many researchers.[2–11] Experiments have been carried out to determine the effects of important factors, such as droplet size, environmental pressure and temperature, and composition of the ambient gas on the combustion characteristics. Theoretical models have also been presented to elucidate the experimental observations and to predict the burning rate and/or lifetime of droplets. Since the fundamental study on the evaporation and chemical reaction processes of LOX in hydrogen-rich environments can be useful in advancing the knowledge of the overall spray combustion, the present work is motivated to explore the transport behavior and structure of a LOX/H_2 diffusion flame at elevated pressures.

Received July 28, 1995; revision received April 2, 1996; accepted for publication April 30, 1996.

*Staff Engineer, Mechanical Engineering Division. Member AIAA.
†Associate Professor, Graduate Institute of Mechanical Engineering. Member AIAA.
‡Distinguished Professor, Department of Mechanical Engineering. Fellow AIAA.

Experimental Apparatus

A gas-pressurized LOX feeding system was used to maintain a stable LOX surface at the exit of the feeding tube (6.35 mm diameter). The chamber pressure was maintained at a prespecified level by a computer feedback-controlled gas supply system. Instead of pure hydrogen, the mixture of helium and hydrogen was employed to pressurize the system for safety considerations. Another reason for using helium is because of its similar solubility features as hydrogen. Direct images of the flame shape of a LOX/hydrogen laminar diffusion flame were recorded using high-magnification video photography. For species concentration measurements, a quartz microprobe with an orifice diameter of 25 μm was used to sample the gas mixture in the postflame region. The gas mixture composition was analyzed using a Varian 3700 gas chromatograph (GC) with a thermal conductivity detector. Detailed description of the experimental setup can be found in Refs. 12 and 13.

Theoretical Approach

A theoretical model[12,13] was formulated to study combustion characteristics of LOX with the H_2/He mixture at elevated pressures. The physical model considers a column of LOX reacting with H_2/He mixture as shown in Fig. 1. Steady-state calculations were performed by considering the LOX being supplied at a certain feeding rate that kept its surface stationary. The gaseous oxygen and hydrogen react and form a stable diffusion flame anchored at the exit of the inner tube. It should be noted that the flame shape can be adjusted to accommodate a range of steady-state flow rates. The governing equations consist of a set of conservation equations of mass, momentum, energy, and species concentrations for a multicomponent system. To allow diffusion in the axial direction, the present analysis treats a fully elliptic problem. The gravitational body force was considered to account for the influence of natural convection. In the treatment of the real-gas behavior, pressure and temperature effects were included for evaluating thermodynamic and transport properties.[14–21] The flame-sheet approximation[22] with consideration of different mass diffusivities (i.e.,

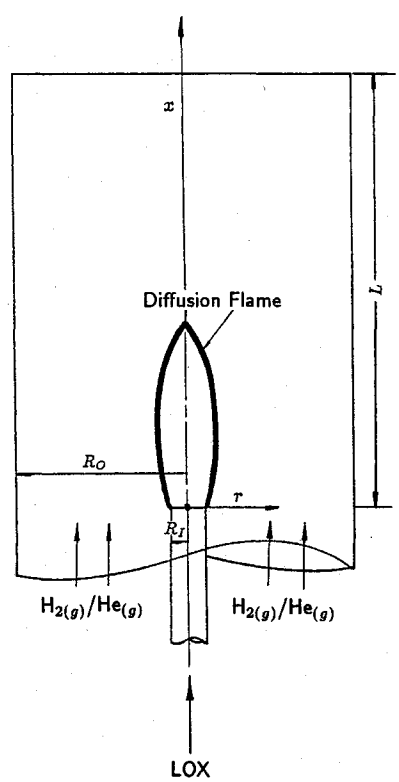

Fig. 1 Schematic diagram of the combustion of LOX with gaseous H_2/He mixture.

nonequal, nonunity *Le*) for various species was used to describe the combustion process of oxygen and hydrogen at high pressures. To characterize the high-pressure solubility of the ambient gas into the liquid, a fugacity-based thermodynamic analysis with quantum-gas mixing rules was also carried out.[23] Calculations were performed by solving the governing equations with an iterative semi-implicit method for pressure-linked equations (SIMPLE) algorithm.[24]

Results and Discussion

In the combustion tests, a stable onion-shape LOX/H_2/He diffusion flame was achieved at a pressure of 30 atm. The laminar diffusion flame studied had an oxygen supply rate of 0.018 gm/s, hydrogen of 0.052 gm/s, and helium of 0.12 gm/s. The LOX surface was below the exit of the feeding tube by about 1.5 mm. When the LOX surface was raised to approach the port of the feeding tube, the flame tended to detach from the tube rim and became unstable. To verify the present axisymmetric steady-state combustion code, a numerical simulation was conducted by considering the LOX surface fixed at the position of 1.5 mm below the exit of the feeding tube. From surface temperature measurements, the LOX surface was 136.2 K at P = 30 atm. The temperature of the surrounding H_2/He was 295 K. Based on measured mass flow rates of oxygen, hydrogen, and helium, the gas velocities of the H_2/He mixture and vaporized LOX were 1.5 and 0.523 cm/s, respectively. The oxygen mass fraction at the LOX surface was also determined to be 0.981 from the phase equilibrium analysis. Figure 2 presents the comparison between predicted and experimentally observed steady flame shape for the coflowing LOX/H_2/He laminar diffusion flame at a pressure of 30 atm. In general, the calculated flame shape was in reasonable agreement with the observed luminous flame surface. The predicted results also matched well with measured radial hydrogen concentration distributions in the stations beyond the flame height (not shown in the figure).[13]

The combustion process of LOX in the surrounding flow of a H_2/He mixture (with a mass ratio of 30/70) at a pressure of 68 atm was also simulated. In the present case considered, the inflow velocity of vaporized oxygen was 0.218 cm/s above the LOX surface, and the flow velocity of the surrounding H_2/He mixture was 1.5 cm/s. The temperatures of the LOX surface and surrounding flow were 153.3 and 295 K, respectively. The phase equilibrium analysis was applied to determine boundary conditions of species concentration at the LOX surface.

Figure 3a shows temperature contours with respect to both axial and radial coordinates. The high-temperature area spanned from the interface region of the oxidizer and fuel inlets near the tube rim to the centerline. The peak temperature along the centerline was about 3310 K. The flame height, defined as the location of the peak centerline temperature, was found to be 1.66 cm above the tube exit. The steep axial temperature gradients were noted in the vicinity of the LOX surface, which indicated a strong heat feedback from the flame to the LOX surface, to provide the energy required in the phase change of oxygen from a compressed liquid to a superheated vapor.

Using the same boundary conditions, another calculation was performed with zero gravity. Figure 3b displays temperature contours without considering the body-force effect. In the case of considering gravity, the buoyancy force accelerates the flow in the reaction zone and thereby increases the entrainment of the surrounding H_2/He mixture. This suction-like effect induces an inward radial flow motion near the port exit plane to enhance combustion and drive the flame closer to the centerline. In contrast to the previous case, the flame core tends to expand in the radial direction and its flame height is taller at the zero-gravity condition. No visible sign of the upward flow acceleration is observed in the high-temperature region.

In diffusion flames, the vorticity field plays an important role in characterizing the mixing and combustion processes. The

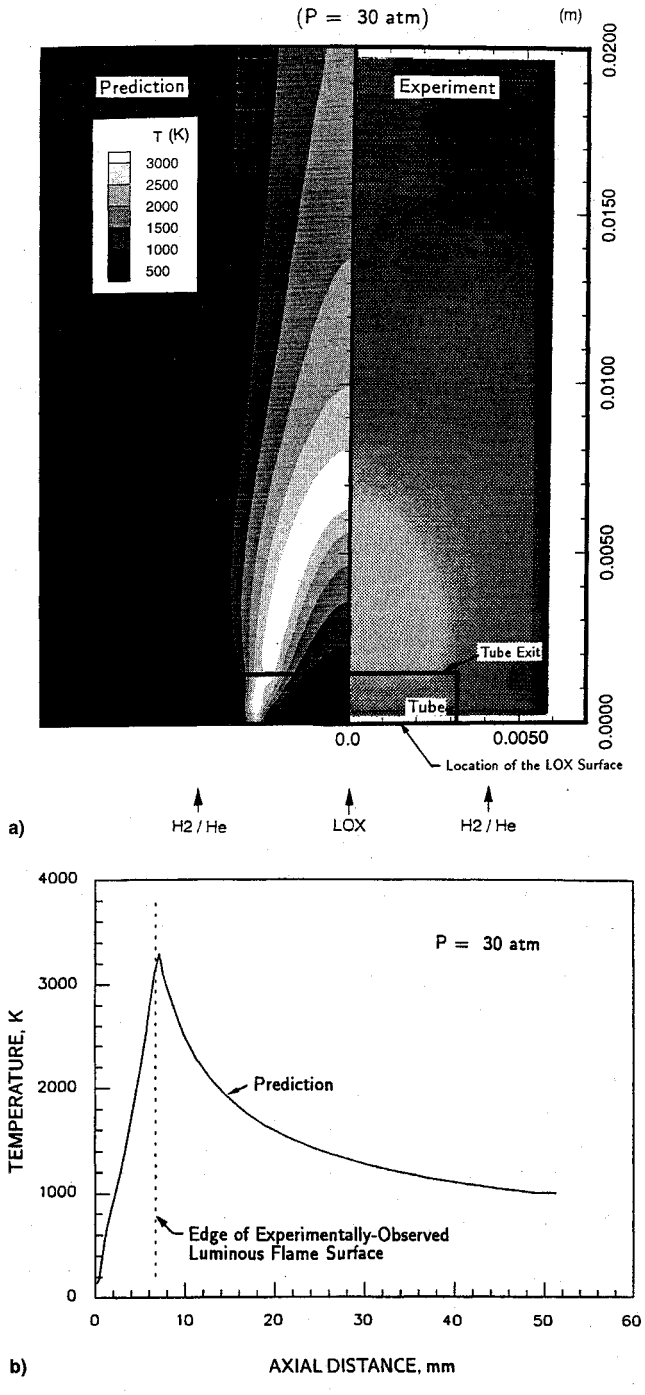

Fig. 2 a) Predicted and experimentally observed flame shape with an oxygen supply rate of 0.018 gm/s at a pressure of 30 atm and b) predicted centerline temperature profile and location of luminous flame surface for the coflowing LOX/H_2/He laminar diffusion flame at a pressure of 30 atm.

rate of change of the vorticity field links to various mechanisms, such as vortex stretching, vorticity dilation, baroclinic torque, and viscous dissipation. In the present two-dimensional axisymmetric analysis, the vortex stretching term disappears. The vorticity dilation is related to the variable density effect for the fluid. The baroclinic torque represents the vorticity generation through a nonalignment of the density and pressure gradients. They are essentially trivial for a nonreacting low-Mach-number flow. However, in combustion situations, these two terms can be significant because of the existence of a strong density variation.

Figure 4 presents the predicted vorticity dilation and baroclinic torque distributions along the centerline above the LOX

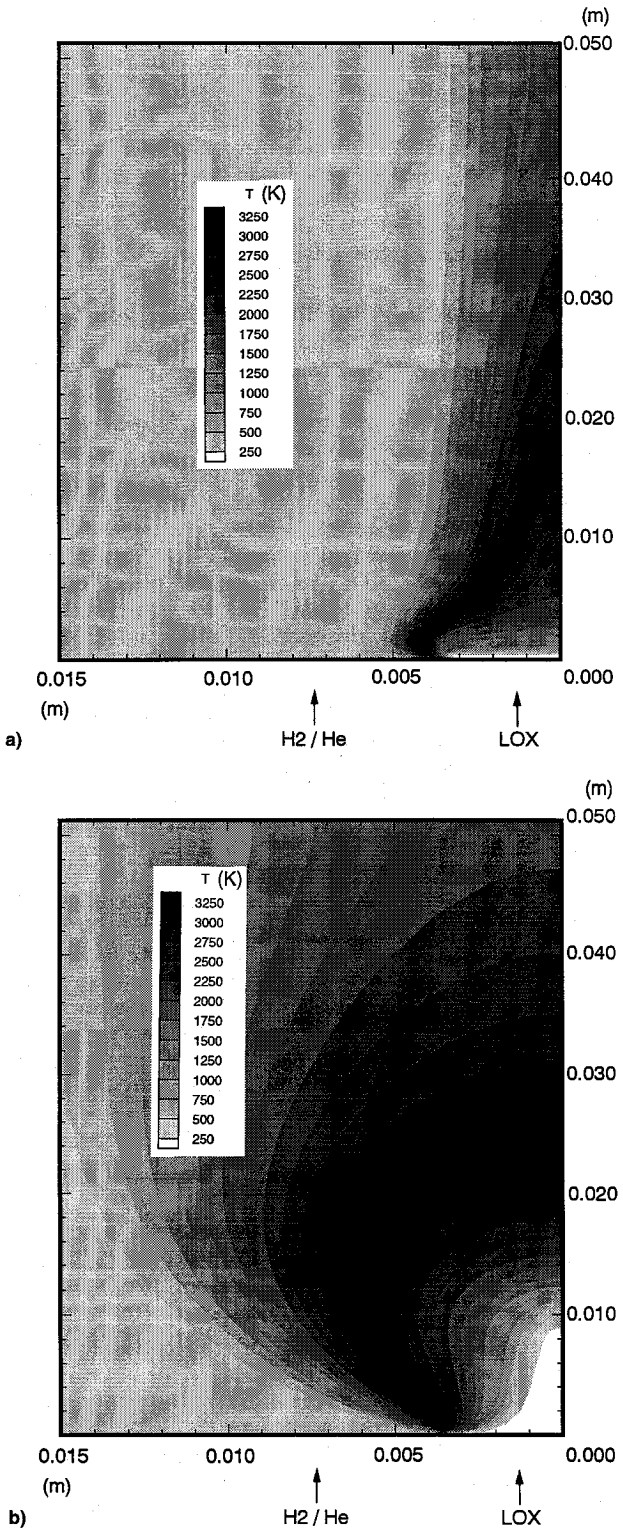

Fig. 3 Temperature contour for the coflowing LOX/H_2/He laminar diffusion flame a) at a pressure of 68 atm and b) without the effect of body force (P = 68 atm).

surface. As shown in the figure, the amplitude of both vorticity dilation and baroclinic torque grew considerably when the exothermic heat took place as a consequence of combustion. This observation also suggested that these two terms could be considered as an indicator of the chemical reaction zone. Moreover, it was noted that the magnitude of the baroclinic torque was substantially larger than that of the vorticity dilation. This indicates that the vorticity field is mainly generated by the misalignment of density and pressure gradients in the flame.

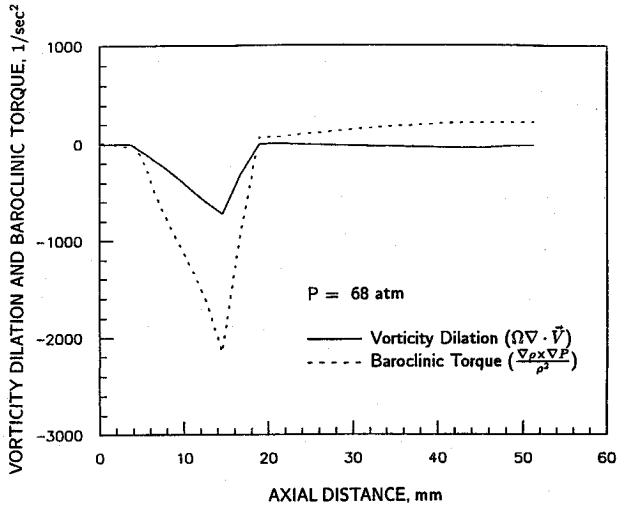

Fig. 4 Predicted centerline vorticity dilation and baroclinic torque distributions for the coflowing LOX/H_2/He laminar diffusion flame (P = 68 atm).

Summary and Conclusions

A theoretical model was formulated and solved numerically to simulate the combustion process of LOX with hydrogen under high-pressure conditions. The model was based on the conservation equations for a multicomponent system, with consideration of gravitational body force, solubility of ambient gases in liquid, and variable thermophysical properties. A fugacity-based thermodynamic analysis with quantum-gas mixing rules was performed to characterize the solubility of ambient gas at the LOX surface. Effect of differential diffusion was considered in the chemical reaction of oxygen with H_2/He mixture at high pressures. A stable onion-shaped LOX/H_2/He diffusion flame was achieved at a pressure of 30 atm. The calculated flame shape agreed well with the shape of the observed luminous flame. Simulation results demonstrated that the development of vortex structure existed in the flame region mainly controlled by the combustion-induced baroclinic torque and buoyancy-driven flow acceleration of the surrounding H_2/He mixture.

Acknowledgments

This research was sponsored by the NASA Marshall Space Flight Center and the Propulsion Engineering Research Center of the Pennsylvania State University. The encouragement and support of Klaus Gross of Marshall Space Flight Center are acknowledged.

References

[1]Sutton, G. P., *Rocket Propulsion Elements*, Wiley, New York, 1986.

[2]Williams, A., "Combustion of Droplets of Liquid Fuels: A Review," *Combustion and Flame*, Vol. 21, 1973, pp. 1–31.

[3]Faeth, G. M., "Current Status of Droplet and Liquid Combustion," *Progress in Energy and Combustion Sciences*, Vol. 3, 1977, pp. 191–224.

[4]Law, C. K., "Recent Advances in Droplet Vaporization and Combustion," *Progress in Energy and Combustion Sciences*, Vol. 8, 1982, pp. 171–201.

[5]Sirignano, W. A., "Fuel Droplet Vaporization and Spray Combustion Theory," *Progress in Energy and Combustion Sciences*, Vol. 9, 1983, pp. 291–322.

[6]Hsieh, K. C., Shuen, J. S., and Yang, V., "Droplet Vaporization in High-Pressure Environments I: Near Critical Conditions," *Combustion Science and Technology*, Vol. 76, 1991, pp. 111–132.

[7]Shuen, J. S., and Yang, V., "Combustion of Liquid-Fuel Droplets in Supercritical Conditions," AIAA Paper 91-78, 1991.

[8]Litchford, R. J., and Jeng, S. M., "LOX Vaporization in High-Pressure, Hydrogen-Rich Gas," AIAA Paper 90-2191, 1990.

[9]Delplanque, J. P., and Sirignano, W. A., "Transient Vaporization and Burning for an Oxygen Droplet at Sub- and Near-Critical Con-

ditions," AIAA Paper 91-75, 1991.
[10]Yang, V., Lin, N. N., and Shuen, J. S., "Vaporization of Liquid Oxygen (LOX) Droplets at Supercritical Conditions," AIAA Paper 92-103, 1992.
[11]Chiu, H. H., and Gross, K. W., "Liquid Behavior at Critical and Supercritical Conditions," JANNAF Workshop Summary, Irvine, CA, 1986.
[12]Yang, A. S., Hsieh, W. H., Kuo, K. K., and Brown, J. J., "Evaporation of LOX Under Supercritical and Subcritical Conditions," AIAA Paper 93-2188, 1993.
[13]Yang, A. S., "Combustion of LOX with H2(g) Under Subcritical and Supercritical Conditions," Ph.D. Dissertation, Pennsylvania State Univ., University Park, PA, 1993.
[14]Sychev, V. V., Vasserman, A. A., Kozlov, A. D., Spiridonov, G. A., and Tsymarny, V. A., *Property Data Update, Official Standards of The National Standard Reference Data Service of the USSR*, Hemisphere, Washington, DC, 1987.
[15]Lucas, K., "Review of Present Status of Transport Properties Predictions," *Phase Equilibria and Fluid Properties in the Chemical Industry*, Dechema, Frankfurt, Germany, 1980, pp. 573–587.
[16]Laesecke, A., Krauss, R., and Stephan, K., "Transport Properties of Fluid Oxygen," *Journal of Physical and Chemical Reference Data*, Vol. 19, No. 5, 1990, pp. 1089–1121.
[17]Chapman, S., and Cowling, T. G., *The Mathematical Theory of Non-Uniform Gases*, Cambridge Univ. Press, New York, 1961.
[18]Takahashi, S., "Preparation of a Generalized Chart for the Diffusion Coefficients of Gases at High Pressures," *Journal of Chemical Engineering of Japan*, Vol. 7, No. 6, 1974, pp. 417–420.
[19]Wilke, C. R., "Diffusional Properties of Multicomponent Gases," *Chemical Engineering Progress*, Vol. 46, No. 2, 1950, pp. 95–104.
[20]Daubert, T. E., and Danner, R. P., *Physical and Thermodynamic Properties of Pure Chemicals: Data Compilation*, Hemisphere, New York, 1989.
[21]McBride, B. J., and Zeleznik, F. J., "Computer Program for Calculation of Complex Chemical Equilibrium Compositions and Applications: Supplement I—Transport Properties," NASA TM-86885, 1984.
[22]Kuo, K. K., *Principles of Combustion*, Wiley, New York, 1986.
[23]Prausnitz, J. M., Lichtenthaler, R. N., and De Azevedo, E. G., *Molecular Thermodynamics of Fluid-Phase Equilibria*, Prentice–Hall, Englewood Cliffs, NJ, 1986.
[24]Patankar, S. V., *Numerical Heat Transfer and Fluid Flows*, Hemisphere, New York, 1980.

Flow Characteristics of a Rectangular Multielement Supersonic Mixer–Ejector

R. Taghavi*
University of Kansas, Lawrence, Kansas 66045
and
G. Raman†
NYMA, Inc., Brook Park, Ohio 44142

Introduction

ONE promising method of supersonic jet noise reduction is the use of a mixer–ejector nozzle.[1–6] The work described in this Note is a part of an ongoing experimental study on the flow physics and performance characteristics of a rectangular multielement supersonic mixer–ejector nozzle. The ejector characteristics studied included the mean flow at the ejector exit, ejector pumping, and the ejector sidewall static pressure. To our knowledge, the only other published work on rectangular supersonic multijet ejectors is that by Chandrasekhara et al.[7] Their results showed that the performance of a multijet ejector is distinctly superior to that of a single equivalent jet ejector. Our main objective is to characterize the performance of multijet ejectors at various primary jet Mach numbers and area ratios (ejector area/primary jet area).

Received April 21, 1995; presented as Paper 95-017 at the AIAA/CEAS 1st Joint Aeroacoustics Conference, Munich, Germany, June 12–15, 1995; revision received Feb. 23, 1996; accepted for publication March 1, 1996.

*Associate Professor, Department of Aerospace Engineering. Senior Member AIAA.
†Senior Research Engineer, NASA Lewis Research Center Group, Experimental Fluid Dynamics Section. Member AIAA.

Experimental Setup and Instrumentation

A schematic diagram of the flow facility used in our experiments is shown in Fig. 1. The facility was previously described in detail in Refs. 8 and 9, therefore, only a brief description is given here. The primary jets emerged from four convergent–rectangular nozzles (6.9 × 34.5 mm) into the straight adjustable-area rectangular ejector. The internozzle spacing (center-to-center) was 6.25 times the narrow dimension of the nozzle. The individual nozzle total pressures were maintained to within ±0.1 psi using an automatic feedback control loop.

The adjustable-area ejector was constructed from Plexiglas® side walls. The leading edges and spacers were made from wood. The total length of the ejector sidewall, in the streamwise direction, was 32.51 cm, which included 5.08 cm of leading edge and 4.45 cm of tapered trailing edge (only the outside surface was tapered). The small dimension of the rectangular ejector could be adjusted by the addition or removal of spacers. The large dimension could be adjusted by loosening the clamps and sliding the small sides (stack of spacers) in or out. The ejector aspect ratio, defined as the ratio of the large to small dimensions of the ejector exit, was kept constant at 4.5 for the two cases studied.

An extra sidewall was fabricated and instrumented with 121 static taps (11 × 11 matrix) connected to the electronic scanning pressure (ESP) modules for instantaneous mapping of the ejector sidewall static pressure distribution. The pressure tap matrix extended from the leading edge to 5.72 cm upstream of the trailing edge. The flow total pressure at the ejector exit was mapped using a pitot probe having an o.d. of 0.8 mm. The probe was traversed over the entire flowfield under computer control.

Results and Discussion

Mean Flowfield at the Ejector Exit

Mach number contours at the ejector exit plane, for two ejector area ratios (AR = 7 and 12) at six primary-jet fully expanded Mach numbers are shown in Fig. 2. The ejector area ratio is defined as the ratio of ejector exit area to the total exit area of the four rectangular nozzles. In these plots, the y and z coordinates are normalized by the primary nozzles' equivalent diameter D_{eq}, defined as the diameter of the circle having an area equal to the total exit area of the four primary rectangular nozzles. From the contour plots of Fig. 2 it is clear that for all primary jet Mach numbers, an increase in the ejector area ratio from 7 to 12 resulted in a reduction in the peak ejector exit Mach number and a more uniform mixing of the primary jets and secondary (ejector entrained) flow.

The ejector pumping per unit secondary area for various cases is plotted in Fig. 3. The pumping was obtained as follows. First the total mass flow at the ejector exit was calculated by integration of the data shown in Fig. 2, then the primary jet's mass flow was subtracted from the total mass flow. Finally the pumping per unit secondary area was calculated. The secondary area is the ejector exit area (constant for an ejector with parallel sidewalls) minus the total exit area of the four primary nozzles. From the plots of Fig. 3 it is clear that, for both area ratios, the ejector pumping per unit secondary area increases when the primary jet Mach number increases. For the case of AR = 7, the variation is almost linear, but the slope decreases as the primary jet Mach number increases beyond